Phonon-induced electron relaxation in quantum rings

G. Piacente* and G. Q. Hai†
Instituto de Fsica de São Carlos, Universidade de São Paulo, 13560-970 São Carlos, São Paulo, Brazil
(Received 18 December 2006; revised manuscript received 15 February 2007; published 27 March 2007)

We study electron–acoustic-phonon scattering and electron relaxation in quantum rings in the absence and in the presence of external magnetic fields. The electron-phonon interaction is accounted for both the deformation potential and piezoelectric coupling. At zero magnetic field and small ring radius, the deformation potential phonon scattering is orders of magnitude larger than the piezoelectric one. However, the piezoelectric coupling is found to become important when the ring radius and magnetic field increase. It can be the dominant scattering mechanism at large ring radii and/or large magnetic fields. In comparison with the quantum dot case, the acoustic phonon scattering is stronger in quantum rings.

DOI: 10.1103/PhysRevB.75.125324 PACS number(s): 63.22.+m, 73.21.La, 73.22.Dj, 71.20.Nr

I. INTRODUCTION

Recent successful fabrication of self-assembled quantum rings (QRs) in nanometer dimensions[1–4] has triggered a great deal of interest in theoretical and experimental research. As a matter of fact, QR structures could lead to the development of novel devices in the fields of quantum cryptography, quantum computation, optics, and optoelectronics. These nanoscale quantum objects also provide an excellent ground to investigate many fundamental physical phenomena such as quantum coherence, which is also critical for quantum information processing.

The study of electron energy relaxation in semiconductor quantum dots (QDs) has received considerable attention[5–8] due to the critical importance of carrier-relaxation processes in the performance of novel semiconductor devices (e.g., lasers and infrared photodetectors) based on QDs. One fundamental question is how the discrete density of electronic states in these nanostructures affects the relaxation time of excited electrons.[9–14] It was recognized that electron-phonon scattering is severely suppressed in QDs.[9,10] In a QD where the energy level separation is small as compared to the optical phonon energy, the electron–acoustic-phonon interaction is dominant.

Electron relaxation in QDs due to acoustic phonon scattering has been studied extensively over the past few years.[5–8] Coupling to acoustic phonons has been effectively proved to be the most important mechanism of electron relaxation from excited states in laterally confined QDs[5,6] and vertically coupled quantum dots (CQDs).[7,8] Both the deformation (DF) potential and the piezoelectric (PZ) acoustic phonons can scatter strongly the excited electrons. These scattering mechanisms have been recently studied for single and coupled QDs.[15–20] Theoretical estimations of phonon-induced scattering rates have shown satisfactory agreement with transport spectroscopy experiments.[2]

In this work, we extend previous calculations of the electron–acoustic-phonon relaxation to the case of quantum rings. In particular, we consider GaAs/AlGaAs QRs. We study single-electron relaxation in a QR as a necessary first step to further investigations of the few-electron and the coupled quantum ring cases. The electron is considered photoexcited or electrically injected to an excited state. The ring is laterally confined, and the effects of the confinement and external magnetic fields are investigated. We took into account both DF and PZ phonon scattering mechanisms, and we stress the differences between the QD and QR geometries. The scattering rate demonstrates strong oscillations as a function of the confinement and the external field.

The outline of our paper is as follows. In Sec. II we present our theoretical model and explain the numerical methods to solve the single-particle problem. In Sec. III we show the numerical calculations of the relaxation rates in the absence and in the presence of magnetic fields, separately. Based on our results, we comment on the differences in the electron relaxation processes between QRs and QDs. Finally, we conclude in Sec. IV.

II. THEORETICAL MODEL

Within the effective mass and envelope function approximation we set up the following model to study the electron relaxation time in QRs. The confinement potential of the QR in the xy plane is modeled by a displaced parabolic function $V(\vec{\mathbf{r}})=m^*\omega_0^2(\vec{\mathbf{r}}_\parallel-r_0)^2/2$, where m^* is the electron effective mass, $\vec{\mathbf{r}}_\parallel\equiv(x,y)$, r_0 is the ring radius, and ω_0 describes the strength of the harmonic confinement in the plane. The confinement potential in the z direction $V_{QW}(z)$ is considered as a quantum well of thickness L_z and barrier height V_0. When a magnetic field $\mathbf{B}$ is applied in the z direction, the Hamiltonian for the single-electron problem is given by

$$H=-\frac{(\vec{\mathbf{p}}+e\vec{\mathbf{A}})^2}{2m^*}+\frac{1}{2}m^*\omega_0^2(\vec{\mathbf{r}}_\parallel-r_0)^2+V_0\Theta(|z|-L_z/2), \tag{1}$$

where $\vec{\mathbf{p}}=-i\hbar\vec{\nabla}$, $\vec{\mathbf{A}}=(-By/2,Bx/2,0)$, $\Theta(z)$ is the Heaviside function, and V_0 is the conduction band offset between the GaAs well and the AlGaAs barrier.

Since the vertical confinement in the z direction is usually much stronger than the lateral one, the in-plane motion and the vertical one can be treated as decoupled. The electron wave function can thereby be written as a product:

$$\psi(\vec{\mathbf{r}}) = \psi_{\parallel}(\vec{\mathbf{r}}_{\parallel})\chi(z), \tag{2}$$

equation where $\vec{\mathbf{r}} \equiv (x,y,z)$. The functions $\psi_{\parallel}(\vec{\mathbf{r}}_{\parallel})$ and $\chi(z)$ describe the electron motion in the xy plane and in the z direction, respectively.

It is known that the present eigenvalue problem of the QR is not analytically solvable. Therefore, we evaluate the matrix elements of the in-plane ring potential on the basis of the two-dimensional parabolic QD—that is, on the Fock-Darwin basis—and diagonalize the corresponding matrix.[21] Thus, the eigenvalues give the energy levels of the in-plane motion and the eigenvector components κ_n^j yield the matrix of the change of basis. The total electron eigenfunction is then a superposition of the Fock-Darwin orbitals

$$\psi_{j,m,g}(\vec{\mathbf{r}}) = \left(\sum_n \kappa_n^j \phi_{n,m}(x,y)\right)\chi_g(z), \tag{3}$$

where $\phi_{n,m}$ is the nth Fock-Darwin orbital with azimuthal angular momentum m and χ_g is the gth finite quantum well solution. The eigenstates can be labeled by the set of three quantum numbers (j,m,g), with $j=0,1,2,\ldots$, $m=0,\pm1,\pm2,\ldots$, and $g=0,1,2,\ldots$, respectively. Throughout this paper we assume that the electron is "frozen" in the lowest-energy state of the quantum well along the z direction, which means that we always consider $g=0$. This assumption is justified by the fact that in normal growth conditions the vertical confinement is much stronger than the in-plane one.

The electron–acoustic-phonon interaction Hamiltonian, disregarding umklapp processes, is given by

$$H_{ep} = \sum_{\vec{\mathbf{q}},\lambda} M_{\lambda}(\vec{\mathbf{q}})(a_{\vec{\mathbf{q}}\lambda}^{\dagger} + a_{\vec{\mathbf{q}}\lambda})\exp(i\vec{\mathbf{q}}\cdot\vec{\mathbf{r}}), \tag{4}$$

where $M_{\lambda}(\vec{\mathbf{q}})$ is the scattering matrix element, $\vec{\mathbf{q}}$ the phonon wave vector, $a_{\vec{\mathbf{q}}\lambda}$ and $a_{\vec{\mathbf{q}}\lambda}^{\dagger}$ the phonon annihilation and creation operators, respectively, and λ the polarization index. At low temperature phonon absorption is negligible. The electron scattering time between the initial state $\psi^i(\vec{\mathbf{r}})$ and the final state $\psi^f(\vec{\mathbf{r}})$ due to phonon emission can be calculated according to the Fermi golden rule,

$$\tau_{if}^{-1} = \frac{2\pi}{\hbar}\sum_{\vec{\mathbf{q}},\lambda} |M_{\lambda}(\vec{\mathbf{q}})|^2 |\langle\psi^f|e^{-i\vec{\mathbf{q}}\cdot\vec{\mathbf{r}}}|\psi^i\rangle|^2 \delta(E_f - E_i - \hbar\,\omega_q), \tag{5}$$

where E_f and E_i stand for the final and initial electron levels, respectively, and $\hbar\omega_q$ is the phonon energy. We study phonon modes with a linear dispersion.

In the considered GaAs semiconductor QR, an electron interacts with the longitudinal acoustic (LA) phonon modes through a deformation potential and with both the longitudinal and the transverse acoustic (TA) phonon modes through piezoelectric fields.[22–25] Thereby, the total scattering matrix element is

$$|M(\vec{\mathbf{q}})|^2 = |M_{\mathrm{LA}}^{\mathrm{DF}}(\vec{\mathbf{q}})|^2 + \sum_{\lambda=\mathrm{LA,TA}} |M_{\lambda}^{\mathrm{PZ}}(\vec{\mathbf{q}})|^2, \tag{6}$$

with the first contribution arising from the deformation potential coupling and the second one from the piezoelectric coupling. Notice that the Hamiltonian of the DF and PZ interactions are real and imaginary, respectively, which allows us to investigate these interactions separately and obtain the total contribution by simply adding up the two rates.[25]

The electron-LA phonon scattering due to the deformation potential is given by[26,27]

$$|M_{\mathrm{LA}}^{\mathrm{DF}}(\vec{\mathbf{q}})|^2 = \frac{\hbar D^2}{2\rho c\Gamma}|\vec{\mathbf{q}}|, \tag{7}$$

where D, ρ, Γ, and c are the deformation potential constant, the crystal density, the volume, and the longitudinal sound velocity, respectively.

For zinc-blende crystals such as GaAs, the only nonvanishing independent piezoelectric constant is h_{14}. The corresponding scattering matrices are given by[26,27]

$$|M_{\mathrm{LA}}^{\mathrm{PZ}}(\vec{\mathbf{q}})|^2 = \frac{32\pi^2\hbar\, e^2 h_{14}^2}{\epsilon_0^2\rho c\Gamma}\frac{(3q_xq_yq_z)^2}{|\vec{\mathbf{q}}|^7}, \tag{8}$$

for the electron–LA-phonon scattering ($\lambda \equiv \mathrm{LA}$), and by

$$|M_{\mathrm{TA}}^{\mathrm{PZ}}(\vec{\mathbf{q}})|^2 = \frac{32\pi^2\hbar\, e^2 h_{14}^2}{\epsilon_0^2\rho c'\Gamma}\left|\frac{q_x^2q_y^2 + q_y^2q_z^2 + q_z^2q_x^2}{|\vec{\mathbf{q}}|^5} - \frac{(3q_xq_yq_z)^2}{|\vec{\mathbf{q}}|^7}\right|, \tag{9}$$

for the electron–TA-phonon scattering ($\lambda \equiv \mathrm{TA}$), where c' is the transversal sound velocity. In the above equations (7)–(9) the phonon dispersions are assumed as $\omega_{q,\mathrm{LA}} = cq$ and $\omega_{q,\mathrm{TA}} = c'q$.

In order to obtain a more tractable form of the piezoelectric coupling, we performed an angular average for the longitudinal and transverse modes separately and then add the terms.[25,28] This approximation leads to a minor quantitative modification on the total scattering rate in comparison with retaining the full $\vec{\mathbf{q}}$ dependence. It will influence neither our main results nor the conclusions in this work. We get the following expression for the electron–piezoelectric-phonon scattering matrix elements:

$$|M^{\mathrm{PZ}}(|\vec{\mathbf{q}}|)|^2 = \frac{\hbar e^2 h_{14}^2}{2\rho c\Gamma}\left(\frac{12}{35} + \frac{1}{\alpha}\frac{16}{35}\right)\frac{1}{|\vec{\mathbf{q}}|} \equiv \frac{\hbar}{2\rho c\Gamma}\frac{P}{|\vec{\mathbf{q}}|}, \tag{10}$$

where we have introduced the constants α and P, which represent the ratio between the longitudinal and transverse sound velocities and the piezoelectric coupling constant, respectively.

In this way, the total electron-phonon scattering matrix element in Eq. (6) becomes

$$|M(\vec{\mathbf{q}})|^2 = \frac{\hbar}{2\rho c\Gamma}\frac{1}{|\vec{\mathbf{q}}|}\left(D^2|\vec{\mathbf{q}}|^2 + P\right). \tag{11}$$

Consequently, the total scattering rate from the (j,m,g) to (j',m',g') state at $T=0$ can be written explicitly as

TABLE I. The GaAs constants used in the paper. Unless otherwise indicated the values are taken from Ref. 29.

Parameter	Symbol	Value
Effective electron mass	m^*	0.067 (m_0)
Crystal density	ρ	5.3×10^3 (kg m^{-3})
Band offset	V_0	3.9×10^{-20} (J)
Longitudinal sound velocity[a]	c	3.7×10^3 (m s^{-1})
Transverse sound velocity[a]	c'	3.2×10^3 (m s^{-1})
Static dielectric constant	ϵ_0	12.8
Deformation potential	D	2.2×10^{-18} (J)
Piezoelectric constant	h_{14}	1.38×10^9 (V m^{-1})
Piezoelectric coupling	P	5.4×10^{-20} (J^2 m^{-2})

[a]Reference 30.

$$\tau^{-1}_{(j,m,g)\to(j',m',g')} = \frac{D^2 q_0^3 + P q_0}{2\pi\rho\hbar\, c^2} \sum_{n'=0}^{N}\sum_{n=0}^{N} \kappa_{n'}^{j'}\kappa_n^j \times \int_0^{\pi/2} d\theta \sin\theta |\langle \phi_{n',m'}| e^{-iq_0 r \sin\theta} |\phi_{n,m}\rangle|^2 \times |\langle \chi_g'| e^{-iq_0 z\cos\theta} |\chi_g\rangle|^2, \quad (12)$$

where $q_0=(E_{j',m',g'}-E_{j,m,g})/\hbar c$ and N is the number of Fock-Darwin orbitals considered. The numerical values of the constants used in the calculations are reported in Table I.

III. NUMERICAL RESULTS AND DISCUSSION

A quantum ring is distinctly different from a dot in that it has a not-simply-connected geometry. This property makes QRs particularly interesting, especially for studies in the presence of a vertical magnetic field.

First of all, we study the energy spectrum for the in-plane motion. In Fig. 1 we show the energy levels as a function of (a) the ring radius at zero magnetic field and (b) the magnetic field at fixed ring radii. The ring radius is measured in units of $\lambda_0=\sqrt{\hbar/m^*\omega_0}$ and the energies in units of $\hbar\omega_0$. For a lateral confinement $\hbar\omega_0=5$ meV, one gets $\lambda_0\sim15$ nm, which is a typical value for the ring radius reported in recent experiments.[31] In Fig. 1(a) we reproduced the results already obtained in Ref. 21 within an identical theoretical framework. We obtained results in perfect agreement with the aforementioned ones, as one can see immediately comparing Fig. 1(a) to Fig. 1 in Ref. 21 in the case of zero magnetic field. Moreover, in the presence of a magnetic field, we calculated the spectra for values of the ring radius other than the ones shown in Fig. 4 of Ref. 21.

It is interesting to notice the differences between the cases $B=0$ and $B\neq0$. In the absence of a magnetic field the lowest states have definite quantum numbers (although the degeneracy $\pm m$ is present). When a vertical magnetic field is present, level crossings occur due to the multiple connected geometry of QRs. The ground state changes from the state with $m=0$ to the ones with $m=-1,-2,-3,\ldots$ with increasing magnetic field [see Fig. 1(b)]. The ring eigenfunctions are piecewise defined as a function of B. This feature is not present in a QD where no level crossings occur between the ground state and the low-lying levels. They converge smoothly to the first Landau levels at large magnetic fields. Actually, identifying the crossing points in the energy spectra in a QR gives straightforward information about the specific ring topology.[32,33] Notice that the crossing point density in magnetic field increases as the ring radius increases.

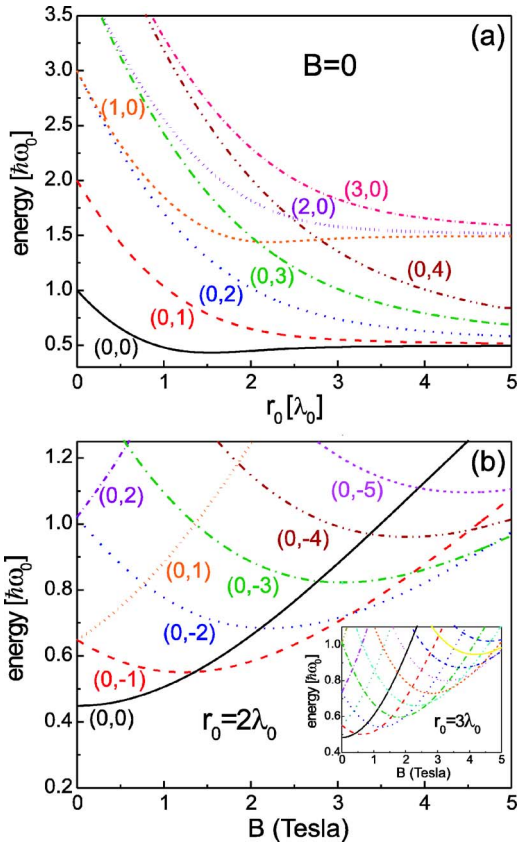

FIG. 1. (Color online) The energy spectrum for the electron in-plane motion as a function of (a) the ring radius at $B=0$ and (b) the magnetic field for $r_0=2\lambda_0$. The inset in (b) shows the spectrum for a ring with $r_0=3\lambda_0$ in the presence of a magnetic field. For $B=0$ the electron levels have the twofold degeneracy $\pm m$.

In what follows, we report calculations of the electron relaxation time due to acoustic phonon scattering in the cases $B=0$ and $B\neq0$. We consider relaxation rates from the first and second excited states to the ground state because they are often the most relevant transitions. These transitions can be monitored experimentally (for instance, by means of pump-and-probe techniques[5,6]). For an electron initially in the first excited state, the relaxation rate is given by the direct scattering rate from this state to the ground state. For electrons in the second (or higher) excited state, different relaxation channels exist and the relaxation rate can be obtained using Matthiessen's rule.

A. In the absence of magnetic field

In this section we study the acoustic phonon scattering and electron relaxation rate in QRs at zero magnetic field. Electron–acoustic-phonon interactions in nanostructures are

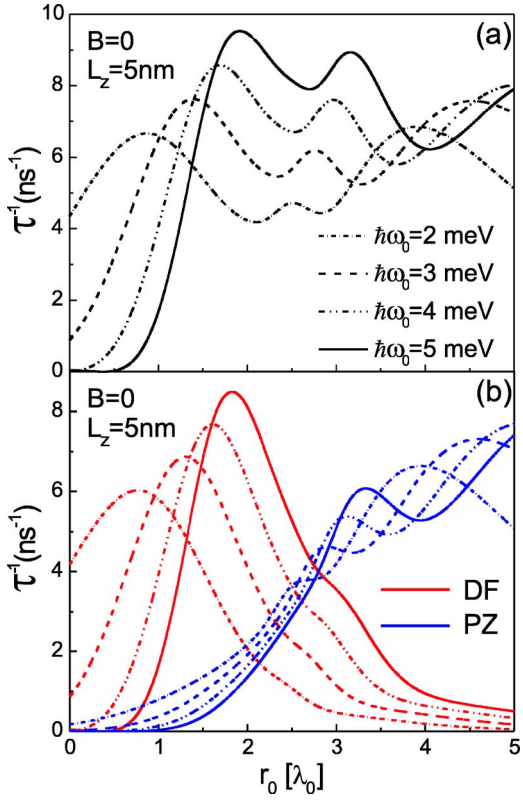

FIG. 2. (Color online) (a) The total scattering rate from the $(0,\pm1,0)$ to the $(0,0,0)$ state as a function of the ring radius for different lateral confinements $\hbar\omega_0$. The vertical well thickness is L_z=5 nm. (b) The contributions of the DF and PZ couplings are plotted separately.

in general determined by the interplay of lateral confinement length, quantum well thickness, and phonon wavelength.[10]

First of all, we calculate the scattering rate as a function of the ring radius r_0 for different lateral confinement frequencies. The scattering rate from the first excited state $(0,\pm1,0)$ to the ground state $(0,0,0)$ is shown in Fig. 2(a) for a fixed ring thickness L_z=5 nm. The scattering rate τ^{-1} shows an oscillatory behavior as a function of the ring radius. For very small r_0 (corresponding to quantum dots), the total scattering rate is small and decreases as the confinement frequency ω_0 increases. With increasing the ring radius, the scattering rate increases pronouncedly for small ω_0. As is evident in Fig. 2(b), for the considered confinement frequencies, the DF acoustic phonon scattering is much larger than the PZ phonon scattering for small ring radius. This is a well-known result for QDs where the DF phonon scattering is dominant.[10] However, our calculation shows that the PZ phonon scattering becomes much larger than that of the DF in QRs (large r_0). For each $\hbar\omega_0$, there is a clear crossover point from which the PZ scattering rate starts to dominate over the DF one. Therefore, in QRs, the PZ effects are important and cannot be neglected as is usually done in QDs. As one can see from Eq. (12), the relative contributions of DF and PZ scattering are determined by the prefactor before the integral. At small q_0 the PZ coupling is dominant over the DF one. Actually, by increasing the ring radius the energy levels get closer and closer [see Fig. 1(a)], and consequently q_0 becomes smaller and smaller. This is the reason why after a certain r_0 the PZ coupling becomes the dominant scattering mechanism. We will return and comment more on this point in the next section.

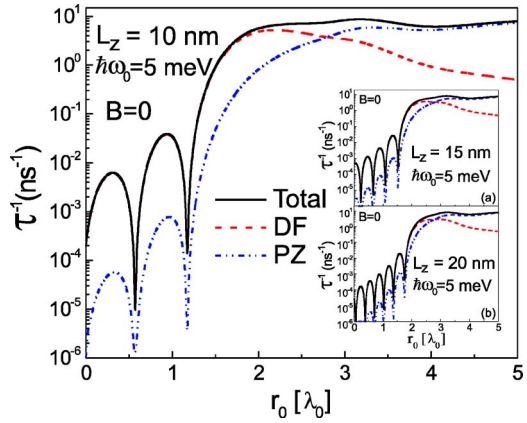

FIG. 3. (Color online) The total, DF, and PZ scattering rates from the $(0,\pm1,0)$ to the $(0,0,0)$ state as a function of the ring radius for different vertical confinements L_z. The lateral confinement is $\hbar\omega_0$=5 meV.

Although the PZ and DF scattering rates are of different features, their behavior in the QD limit (i.e., $r_0\rightarrow0$) is similar. They decreases rapidly as the lateral confinement frequency increases. The reason is that the orthogonality of the electron states leads the factor $\langle\psi^f|\exp(-i\vec{\mathbf{q}}\cdot\vec{\mathbf{r}})|\psi^i\rangle$ to vanish rapidly when the phonon wavelength is shorter than the lateral confinement length.[10]

In Fig. 3, the effect of the QR thickness L_z on the phonon scattering rates is studied. The DF and PZ, as well as total scattering rates, are given as a function of the ring radius for three different L_z at fixed lateral confinement $\hbar\omega_0$=5 nm. The scattering curves exhibit strong oscillations for small ring radius. The oscillation in the electron-phonon scattering rate originates from the match of the localized electron wavelength to the wavelengths of the emitted phonons in the scattering as discussed in Ref. 10 for the QD case. In the calculation, the electron wave function is decoupled in the z direction and in the xy plane. Thus, such a match depends on the projection of the phonon wave vector onto the xy plane due to its three-dimensional (3D) characteristic. For large L_z, the electron-phonon scattering elements depend more strongly on the projection angle of the phonon wave vector onto the xy plane. Consequently, the oscillation in the scattering rate is stronger for larger L_z. It reaches maxima (minima) when the electron wave function is in-phase (antiphase) with the phonon wave. The scattering rate can be suppressed by orders of magnitude due to the antiphase relation between the electron wave function and the phonon wave in the ring. This effect has been proposed as a possible way to control the coherence time for single and coupled QDs.[15,18,19] With increasing ring radius, the phonon scattering is enhanced pronouncedly and the oscillations disappear.

We calculated the relaxation rates τ_r^{-1} for the transitions from the first and second excited states to the ground state as shown in Fig. 4 for the QRs with $\hbar\omega_0$=5 meV and L_z=5 nm. For an electron in the first excited state $(0,\pm1,0)$,

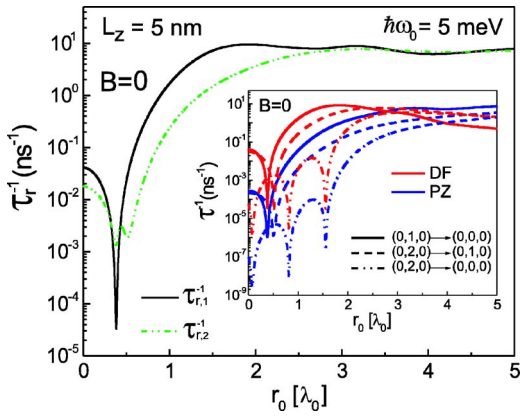

FIG. 4. (Color online) The relaxation rates for the transitions from the first excited state and the second excited state to the ground state as a function of the ring radius. The inset shows the DF and PZ scattering time for all transitions involved in the relaxation processes.

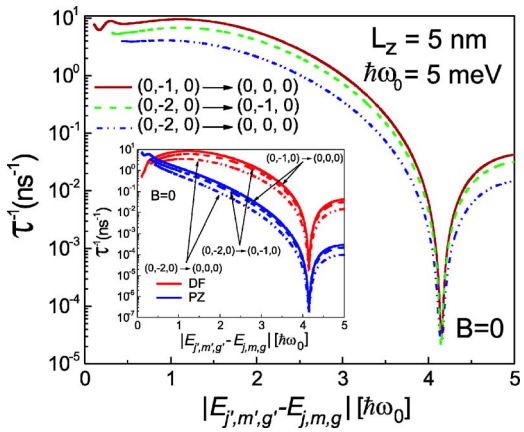

FIG. 5. (Color online) The scattering rate for the transitions between two low-lying adjacent states as a function of the energy difference of the two levels. In the inset the DF and PZ contributions for all possible transitions are given separately.

its relaxation rate $\tau_{r,1}^{-1}$ to the ground state coincides with the direct scattering rate between the two states, as already mentioned. For an electron in a higher state, its relaxation to the ground state is in general a multichannel process. In the specific case under investigation, an electron in the second excited state $(0,\pm 2,0)$ can relax to the ground state by direct transition $(0,\pm 2,0)\rightarrow(0,0,0)$ or indirect transition $(0,\pm 2,0)\rightarrow(0,\pm 1,0)\rightarrow(0,0,0)$. Using Matthiessen's rule, the relaxation rate for the second excited state can be written as

$$\tau_{r,2}^{-1} = \tau_{(0,\pm 2,0)\rightarrow(0,0,0)}^{-1} + (\tau_{(0,\pm 2,0)\rightarrow(0,\pm 1,0)} + \tau_{(0,\pm 1,0)\rightarrow(0,0,0)})^{-1}. \tag{13}$$

From Fig. 4 one can notice that for a large ring radius the two relaxation rates $\tau_{r,1}^{-1}$ and $\tau_{r,2}^{-1}$ are very similar and of the order of 10 ns^{-1}. For a small ring radius, interesting features appear. The relaxation rate $\tau_{r,1}^{-1}$ shows a striking dip at $r_0 \sim 0.38\lambda_0$, and $\tau_{r,2}^{-1}$ has two minima at $r_0 \sim 0.38\lambda_0$ and $r_0 \sim 0.52\lambda_0$ where the relaxation rate is reduced by orders of magnitude. This effect results from the antiphase relation between the electron and phonon wave functions as discussed above. Although it is extremely difficult to control the QR geometry in the fabrication process, in the same spirit of Refs. 15, 18, and 19 we can affirm that a geometry-induced control of the relaxation time is feasible also in the case of QRs of small radius.

The inset of Fig. 4 provides us with some extra information: the DF coupling is more efficient than the PZ one in the relaxation processes from higher excited states with respect to the first excited state. In other words, the crossing where the PZ scattering starts to dominate over the DF one in the transitions $(0,\pm 2,0)\rightarrow(0,0,0)$ and $(0,\pm 2,0)\rightarrow(0,\pm 1,0)$ takes place at a larger r_0 than that in the transition $(0,\pm 1,0)\rightarrow(0,0,0)$.

To conclude this subsection, we plot in Fig. 5 the scattering rates for the transitions $(0,\pm 1,0)\rightarrow(0,0,0)$, $(0,\pm 2,0)\rightarrow(0,\pm 1,0)$, and $(0,\pm 2,0)\rightarrow(0,0,0)$ as a function of the energy difference between the corresponding levels [i.e., the emitted phonon wave number $q_0=(E_{j',m',g'}-E_{j,m,g})/\hbar c$] instead of the ring radius. Though the scattering rate is strongly dependent on the initial and final states, it is evident from Fig. 5 that the scattering rates for the same q_0 are very similar. This indicates that a crucial quantity in the scattering process is the energy difference between the ring levels or q_0. Furthermore, strong scattering occurs at small q_0 (i.e., long-wavelength phonons) where the relaxation time is on the order of 0.1 ns. As one can see from the inset, the PZ and DF phonon scattering in this region is of approximatively the same contribution. This again confirms that differently from the QD case, the PZ phonon scattering is critical in the QRs. The scattering rate decreases rapidly with increasing q_0, and the DF phonon scattering becomes dominant over the PZ one (about two orders of magnitude). Strong scattering at small energies implies that the transition probability for an electron from one state to its adjacent level in energy is much larger than to other levels. As a consequence, relaxation from a higher excited state to the ground state is basically a multiscattering process through all the intermediate states between them.

B. In the presence of a magnetic field

In this section we study the effects of a magnetic field B on the electron-phonon scattering and the electron relaxation time in a QR. As shown in Fig. 1(b), an external magnetic field in the z direction alters drastically the electron energy spectrum.

For instance, the ground state in the case $r_0=2\lambda_0$ is defined by the orbitals $(0,0,0)$ for $0\leqslant B<1.35$, $(0,-1,0)$ for $1.35\leqslant B<3.14$, $(0,-2,0)$ for $3.14\leqslant B<4.77$, and so on. Hence, the ring eigenstates as a function of magnetic field are piecewise. In Ref. 34 the effect of a time-varying magnetic field is shown to produce nonadiabatic changes upon the electron states of the QR, leading to strong nonlinear effects in the time-dependent magnetization.

In what follows, we will refer to the ground state and the first and second excited states as G.S., F.E.S., and S.E.S.,

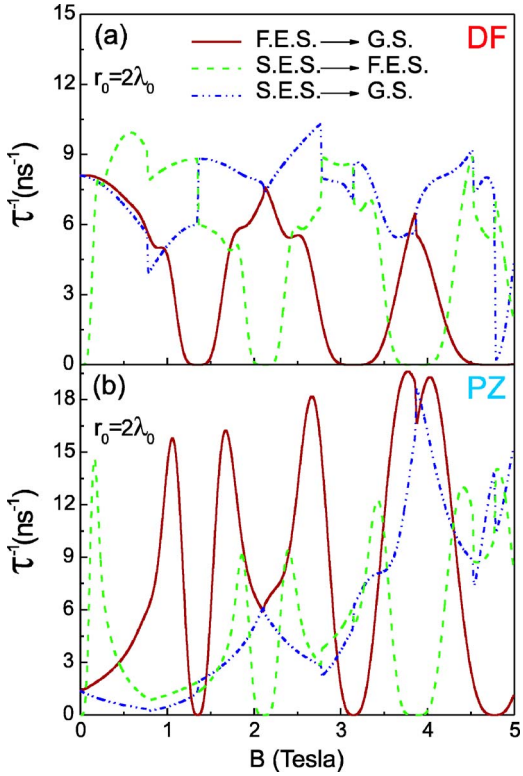

FIG. 6. (Color online) The scattering rates as a function of the magnetic field for a ring of radius $r_0=2\lambda_0$ for (a) the DF and (b) the PZ couplings.

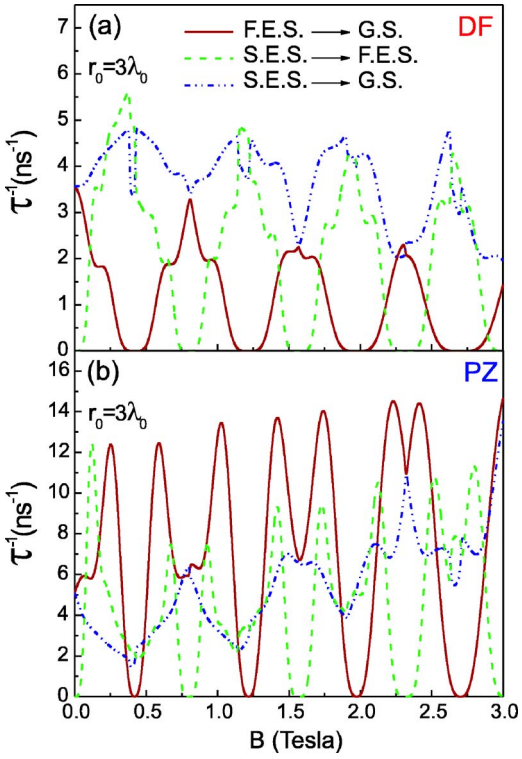

FIG. 7. (Color online) The same as Fig. 6, but with $r_0=3\lambda_0$.

respectively, rather than as a set of three quantum numbers. From now on we concentrate on a well-defined ring geometry with $L_z=5$ nm and $\hbar\omega_0=5$ meV. For fixed ring radii $r_0=2\lambda_0$ and $r_0=3\lambda_0$, we calculated the scattering rates among the lowest three states (i.e., the S.E.S., F.E.S., and G.S.) as a function of magnetic field. The results are shown in Figs. 6 and 7, respectively. The contributions of the DF and PZ phonons to the scattering rates are given separately.

The first notable feature is that the scattering rates due to the PZ and DF phonons have approximatively the same order of magnitude in magnetic fields. Therefore, for QRs in the presence of B we cannot disregard any one of the two scattering mechanisms. In order to describe properly the phonon scattering processes in the QRs in magnetic fields, inclusion of the PZ interaction is fundamental. In fact, as is evident in Figs. 6 and 7, the PZ scattering is almost twice larger than the DF one for the transition F.E.S. → G.S. Actually, the presence of a magnetic field produces a similar effect as increasing the ring radius; that is, it draws the energy levels up, reducing in this way the value of q_0 and, consequently, enhancing the relative importance of the PZ coupling.

The highest scattering rates in a small ring ($r_0=2\lambda_0$) are larger than those in a larger ring ($r_0=3\lambda_0$). Furthermore, the scattering rates oscillate more as a function of B in the ring of $r_0=3\lambda_0$. This is strictly related to the increasing number of level crossings as r_0 becomes larger. Notice that in this case the oscillations are due to the in-plane level crossings at which $q_0\rightarrow 0$ rather than to the antiphase relation between the electron and phonon wave functions in the QD case.[15]

It is interesting to make a direct comparison with the QD case. In Fig. 8 the different scattering contributions are calculated for a QD with $\hbar\omega_0=5$ meV and $L_z=5$ nm in vertical magnetic fields—i.e., the same thickness and confinement frequency as the ring studied above. For magnetic fields up to 5 T, the PZ phonon scattering rates in the QD are always orders of magnitude smaller than the DF ones, as one can see in Fig. 8. Once more, this confirms that the phonon scattering mechanism in QRs is significantly different the QDs. Such a difference is amplified in the presence of magnetic fields. In the QDs, the PZ phonon scattering can be neglected in the presence of B. In the QRs, on the contrary, the PZ interactions are as important as the DF ones.

In Figs. 9 and 10 we show the relaxation rates from the F.E.S. to G.S. and from the S.E.S. to G.S. as a function of B

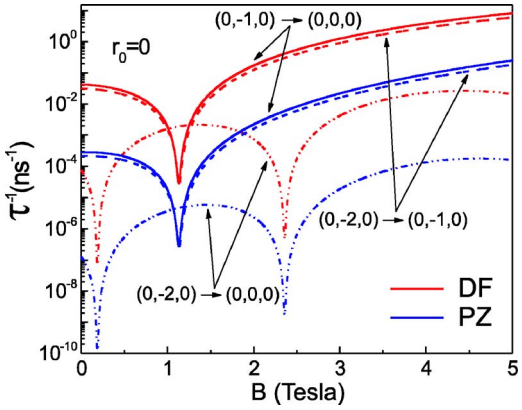

FIG. 8. (Color online) The scattering rates as a function of magnetic field in the case of a quantum dot.

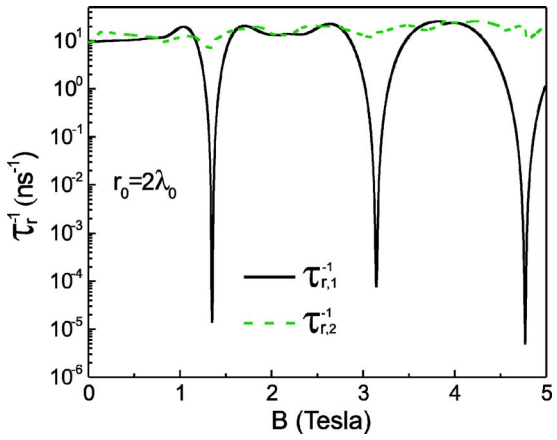

FIG. 9. (Color online) The relaxation rate for the transitions from F.E.S. to G.S. and the S.E.S. to G.S. as a function of magnetic field for a ring of radius $r_0=2\lambda_0$.

for $r_0=2\lambda_0$ and $r_0=3\lambda_0$, respectively. In both cases the relaxation rate from the F.E.S. to G.S. shows dips at the level crossings between the two states, where the phonons (with $q_0\rightarrow 0$) involved in the scattering are of vanishing density of states. This mechanism is distinctly different from the suppression of the scattering rate due to the antiphase relation between the electron and the phonon wave functions as was shown in Fig. 4.

Variation of the relaxation rate from the second excited state to the ground state in magnetic fields is quite small and no dips appear. The reason is that $\tau_{r,2}^{-1}$ results from a multiscattering process and it is calculated according to Matthiessen's rule in Eq. (13). Due to the fact that the crossing points in the energy levels for the G.S., F.E.S., and S.E.S. take place at different magnetic fields, the direct scattering rates $\tau_{\text{F.E.S.}\rightarrow\text{G.S.}}^{-1}$, $\tau_{\text{S.E.S.}\rightarrow\text{F.E.S.}}^{-1}$, and $\tau_{\text{S.E.S.}\rightarrow\text{G.S.}}^{-1}$ are never zero simultaneously.

Finally, in Fig. 11 we show the total scattering rates in the presence of B between two different levels as a function of the energy difference between the corresponding levels instead of magnetic field. Both the DF and PZ phonons are included. We observe that the scattering rates in magnetic fields depend strongly on the energy difference between the levels considered. But at the same energy difference, the different scattering rates are in the same order of magnitude, independently of the initial and final states. Furthermore, when we compare Figs. 11(a) and 11(b) of different ring radii (see also Fig. 5), we find that the curves in the different figures are very similar to each other; i.e., the values of the scattering rates and the positions of the maximum and minimum are almost the same. We can, thereby, confirm that the energy difference between the two states involved in the transitions is a crucial parameter in determining the acoustic phonon scattering rates. Changing the ring radius and/or the magnetic field affects essentially the energy separation between different levels and, consequently, the phonon scattering rate.

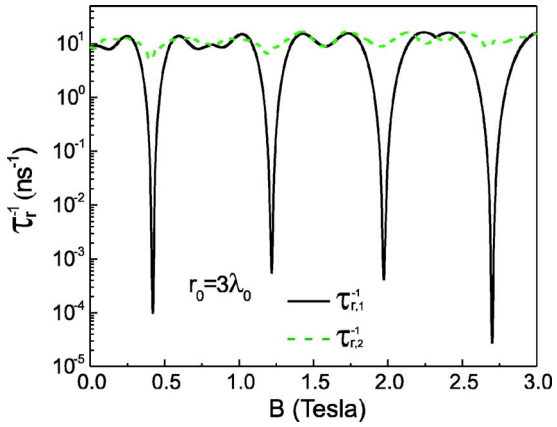

FIG. 10. (Color online) The same as Fig. 9 but for $r_0=3\lambda_0$.

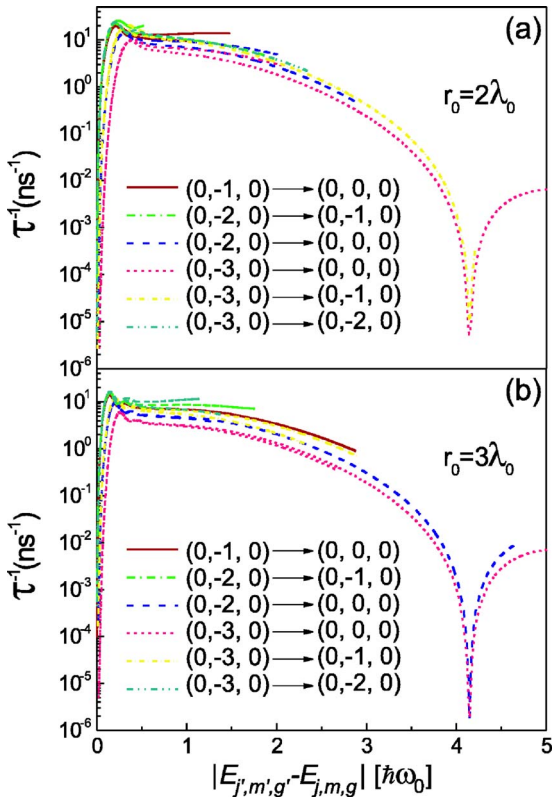

FIG. 11. (Color online) The scattering rates in the presence of a vertical magnetic field for the transitions between the different levels defining the low-lying ring states as a function of the energy differences. In (a) is depicted the case $r_0=2\lambda_0$ and in (b) the case $r_0=3\lambda_0$. Notice the similarity with Fig. 5.

IV. CONCLUSIONS

We studied the acoustic-phonon-induced relaxation of an excited electron in a single GaAs quantum ring. We investigated the effects of the ring geometry and external magnetic fields on the relaxation from the first and second excited states to the ground state. Our calculations show that electron-phonon scattering strongly depends on the ring lateral and vertical dimensions and on the external fields. We took into account both the deformation potential and piezoelectric field couplings and showed that they both give important contributions to the electron relaxation. The piezo-

electric interaction, which is often negligible in quantum dots, represents the major source of scattering in quantum rings of large ring radius or when a high magnetic field is applied. For small ring radii, the deformation potential coupling prevails, being similar to the quantum dot case. Nevertheless, we have shown that the electron-phonon scattering rate between any two levels is mainly determined by the energy difference between them. In magnetic fields, a multiple-scattering process leads to a relaxation time on the order of 10^{-1} ns for an electron from the second excited state to the ground state in QRs.

ACKNOWLEDGMENTS

This work was supported by FAPESP and CNPq, Brazil.

*Electronic address: gpiacente@ursa.usp.br
†Electronic address: hai@ifsc.usp.br

[1] J. M. Garcia, G. Medeiros-Ribeiro, K. Schmidt, T. Ngo, J. L. Feng, A. Lorke, J. P. Kotthaus, and P. M. Petroff, Appl. Phys. Lett. **71**, 2014 (1997).
[2] A. Lorke, R. J. Luyken, A. O. Govorov, J. P. Kotthaus, J. M. Garcia, and P. M. Petroff, Phys. Rev. Lett. **84**, 2223 (2000).
[3] D. Mailly, C. Chapelier, and A. Benoit, Phys. Rev. Lett. **70**, 2020 (1993).
[4] T. Mano, T. Kuroda, S. Sanguinetti, T. Ochiai, T. Tateno, J. Kim, T. Noda, M. Kawabe, K. Sakoda, G. Kido, and N. Koguchi, Nano Lett. **5**, 425 (2005).
[5] T. Fujisawa, D. G. Austing, Y. Tokura, Y. Hirayama, and S. Tarucha, Nature (London) **419**, 278 (2002).
[6] T. Fujisawa, D. G. Austing, Y. Tokura, Y. Hirayama, and S. Tarucha, J. Phys.: Condens. Matter **15**, R1395 (2003).
[7] T. Fujisawa, T. H. Oosterkamp, W. G. van der Wiel, B. W. Broer, R. Aguado, S. Tarucha, and L. P. Kouwenhoven, Science **282**, 932 (1998).
[8] G. Ortner, R. Oulton, H. Kurtze, M. Schwab, D. R. Yakovlev, M. Bayer, S. Fafard, Z. Wasilewski, and P. Hawrylak, Phys. Rev. B **72**, 165353 (2005).
[9] U. Bockelmann and G. Bastard, Phys. Rev. B **42**, 8947 (1990).
[10] U. Bockelmann, Phys. Rev. B **50**, 17271 (1994).
[11] N. Mori and T. Ando, Phys. Rev. B **40**, 6175 (1989).
[12] M. A. Stroscio, Phys. Rev. B **40**, 6428 (1989).
[13] K. W. Kim and M. A. Stroscio, J. Appl. Phys. **68**, 6289 (1990).
[14] K. W. Kim, M. A. Stroscio, A. Bhatt, V. V. Mitin, and R. Mickevicius, J. Appl. Phys. **70**, 319 (1991).
[15] J. I. Climente, A. Bertoni, G. Goldoni, and E. Molinari, Phys. Rev. B **74**, 035313 (2006).
[16] V. N. Stavrou and X. Hu, Phys. Rev. B **72**, 075362 (2005).
[17] Z. J. Wu, K. D. Zhu, X. Z. Yuan, Y. W. Jiang, and H. Zheng, Phys. Rev. B **71**, 205323 (2005).
[18] A. Bertoni, M. Rontani, G. Goldoni, F. Troiani, and E. Molinari, Appl. Phys. Lett. **85**, 4729 (2004).
[19] A. Bertoni, M. Rontani, G. Goldoni, F. Troiani, and E. Molinari, Physica E (Amsterdam) **26**, 427 (2004).
[20] G. Q. Hai and S. S. Oliveira, Appl. Phys. Lett. **88**, 196101 (2006); Phys. Rev. B **74**, 193303 (2006).
[21] J. Simonin, C. R. Proetto, Z. Barticevic, and G. Fuster, Phys. Rev. B **70**, 205305 (2004).
[22] P. J. Price, Surf. Sci. **113**, 119 (1982); **143**, 145 (1984).
[23] E. E. Mendez, P. J. Price, and M. Heiblum, Appl. Phys. Lett. **45**, 294 (1984).
[24] W. Walukiewicz, H. E. Ruda, J. Lagowski, and H. C. Gatos, Phys. Rev. B **29**, 4818 (1984).
[25] G. D. Mahan, *Many-Particle Physics* (Plenum Press, New York, 1990).
[26] P. Vogl, *Physics of Nonlinear Transport in Semiconductor* (Plenum Press, New York, 1980).
[27] J. Zhou, J. L. Cheng, and M. W. Wu, Phys. Rev. B **75**, 045305 (2007).
[28] J. D. Zook, Phys. Rev. **136**, A869 (1964).
[29] J. S. Blakemore, J. Appl. Phys. **53**, R123 (1982).
[30] The values of sound velocities are averages between the bulk and the surface velocity; in this way, both the bulk and the confined acoustic phonon modes are taken into account. For the numeric values of c and c' see, e.g., R. Ferreira and G. Bastard, Phys. Rev. B **40**, 1074 (1989); H. Bruus, K. Flensberg, and H. Smith, *ibid.* **48**, 11144 (1993).
[31] A. Emperador, M. Pi, M. Barranco, and A. Lorke, Phys. Rev. B **62**, 4573 (2000).
[32] A. Fuhrer, S. Lüscher, T. Ihn, T. Heinzel, K. Ensslin, W. Wegschel, and M. Bichler, Nature (London) **413**, 822 (2001).
[33] J. I. Climente, J. Planelles, and J. L. Movilla, Phys. Rev. B **70**, 081301(R) (2004).
[34] V. Gudmundsson, C. S. Tang, and A. Manolescu, Phys. Rev. B **67**, 161301(R) (2003).